

Metabasin Analysis of the Stress Overshoot in Sheared Supercooled Liquids

Markus Blank-Burian^{1,*} and Andreas Heuer¹

¹*Institute for Physical Chemistry
Westfälische Wilhelms-Universität Münster, Germany*

Abstract

Understanding the yielding of amorphous systems upon shearing is notoriously difficult since it is a strong non-equilibrium effect. Here we show that the concept of the potential energy landscape (PEL), developed for the quiescent state, can be extended to shearing. When introducing an appropriate coarse graining of the extended PEL for sheared systems, one can distinguish two fundamentally different types of plastic events, namely inherent structures (IS) vs. minimized structure (MS) transitions. From the properties of the MS transitions one can clearly distinguish between the onset of irreversible plastic events and the stress overshoot. Furthermore, the potential energy, required to reach the stress overshoot, is directly related to energies, relevant for the description of the quiescent system.

Introduction. A common feature of amorphous glass forming materials like metallic glasses, colloidal particles or foams is an overshoot in the stress-strain curve when applying a constant shear rate when starting at rest. During this overshoot period, the material performs a transition from solid-like to fluid-like behavior.

It has been the focus of recent work to study the process of yielding in more detail [1–8]. The simplest approach of defining a *yield strain* γ_y in glasses is taking the strain at the maximum. Another approach [5] uses an overlap function to determine whether there has been a larger rearrangement between two configurations. The yield is then defined as the point where half of the systems had such a transition. The same results are obtained by using susceptibilities [9]. When using oscillatory shear also the equality of the storage modulus G' and the loss modulus G'' can be used to characterize the transition from elastic to non-elastic behavior. This rheological crossover strain is again close to γ_y and also related to a sharp transition in the anisotropy of the structure factor [8].

Interestingly, via oscillatory shear experiments and simulations in the low-temperature limit a second smaller *critical strain* γ_{nl} can be defined, marking the onset of non-linear behavior [10–12]. Whereas for strain amplitudes $\gamma_{max} < \gamma_{nl}$ one observes limit cycles of the trajectory [1, 6, 10, 12], for $\gamma_{max} > \gamma_{nl}$ the system irreversibly leaves its initial region of configuration space. Whereas γ_y only has a small dependence on system size, the value of γ_{nl} , reported in [10], decreases from 0.115 to 0.070 when increasing the system size from $N = 500$ to $N = 32000$.

Already for strain values significantly below the yield strain, plastic events do occur. This raises the vital question, which plastic events finally give rise to the critical strain and the yield strain, respectively. More generally one can ask where irreversibility really starts. To approach these questions, we will employ a new method of detecting transitions using the framework of the potential energy landscape (PEL). For this purpose we analyse the properties in the extended PEL $V(\mathbf{x}, \gamma)$, depending on the configuration \mathbf{x} as well as the external strain γ . The key idea is to study minima with respect to all $3N + 1$ variables which are relevant for the dynamics. This allows us to define two different types of plastic events. Based on this information we can map the two different yield strains to the underlying properties of the PEL.

Technical aspects. We use a slightly modified form of the standard binary mixture of

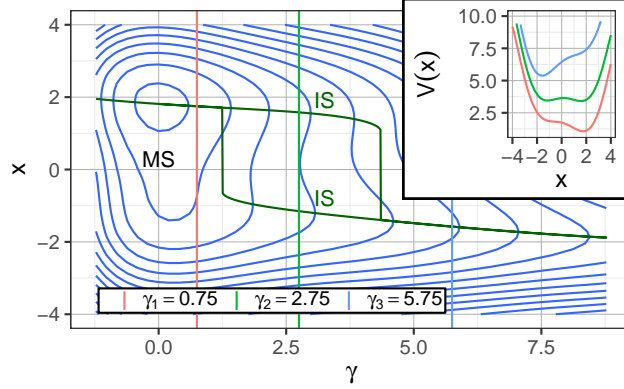
Lennard-Jones particles [13] with a cutoff of $r_c = 1.8$ in our 3D molecular dynamics (MD) simulations. Since the potential energy shows saddle-node bifurcations [14], we took care to make the potential continuous up to the second derivative at the cutoff. For this purpose we multiply the potential with a polynomial of 5th order in the range $r \in [0.9r_c, r_c]$ which has no effects on the observables discussed below. For the shearing we used Lees-Edwards boundary conditions [15] together with the SLLOD algorithm [16].

For the quiescent case ($\dot{\gamma} = 0$) the system mainly resides close to the minima of the PEL for $T \leq 0.7$ [17], interrupted by fast jumps between them. Starting with a configuration at $\gamma = 0$, the associated inherent structure (IS) can be found by minimizing the potential energy $V(\mathbf{x})$ starting with the current particle positions $\mathbf{x}(t)$ in the trajectory [18]. Its energy is denoted ϵ_{IS} . Furthermore, adjacent IS can be combined into a metabasin (MB) [19, 20]. Its energy ϵ_{MB} is characterized by the minimum IS energy within this MB, corresponding to the representative MB configuration.

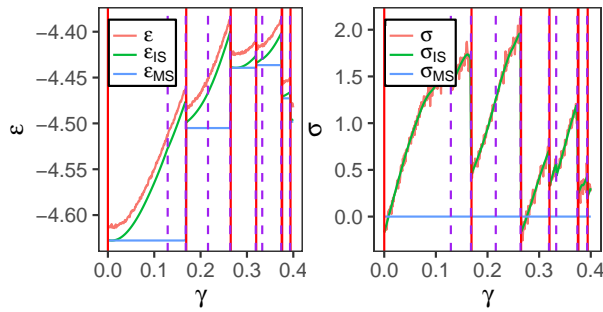
To prepare starting structures for the shearing simulations deep in the glass, we first performed equilibrium simulation runs at $\gamma = 0$ and $T \geq 0.435$ in order to generate different MB configurations. For runs constrained to a specific starting MB energy ϵ_{start} , we allowed deviations by at most 0.01. At $\epsilon_{\text{start}} \geq -4.6$ we used at least 128 independent starting configurations. All other runs used a selection of starting configurations with $\langle \epsilon_{\text{start}} \rangle = -4.6$. We always mention the average energy per particle.

A quantitative PEL analysis requires the use of small systems [21]. In the standard view, as employed, e.g., in the elasto-plastic models [22], the overall response is the effect of local plastic events and the subsequent mutual elastic coupling. The simulation of small systems allows one to identify the elementary plastic events. A similar reasoning has been used before for the quiescent case where the study of small systems together with a model for the elastic coupling could explain several non-trivial features of large systems, such as the time-temperature superposition [23]. If not mentioned otherwise, we used $N = 130$ particles for our simulations.

PEL under shear. When shearing the system at low temperatures, the configuration closely follows the current local potential energy minimum, defined in the complete potential energy $V(\mathbf{x}, \gamma)$ as also expected for athermal quasistatic shear (AQS) simulations [14, 24]. For some strain value the barrier disappears and the system experiences a plastic event,



(a)



(b)

(c)

FIG. 1. (a) Illustration of the minimization routine for a 1D potential, shown for different strain values. Displayed are the contours of a specifically designed 6th order polynomial. The solid lines show the taken paths where the inherent states would evolve by increasing/decreasing the strain. The vertical lines mark the strain values, for which the potential is plotted in the inset. (b) Energy at the start of a shear simulation, starting at $\epsilon \approx -4.65$ with $T = 0.01$, $N = 130$. Dashed/Solid vertical lines mark the detected transitions between inherent structures (IS) / minimized structures (MS). (c) Stress of the inherent structures for the same simulation.

thereby reducing its stress. On a qualitative level the shearing can be visualized as a tilting of the PEL [14] and a subsequent fold-catastrophe [25].

Our goal is to describe these processes in the extended PEL, based on $V(\mathbf{x}, \gamma)$. The dependence of the potential energy on the strain γ results from the use of Lees-Edwards boundary conditions. For illustration purposes we first discuss a toy PEL $V(\mathbf{x}_{\text{IS}}, \gamma)$ with just one real-space coordinate \mathbf{x}_{IS} ; see FIG. 1a. An example trajectory is included which, for given γ , is always at the local minimum with respect to the spatial coordinate \mathbf{x}_{IS} , i.e. in an IS. As the strain is increased, its coordinate changes and the energy increases. At some strain value the

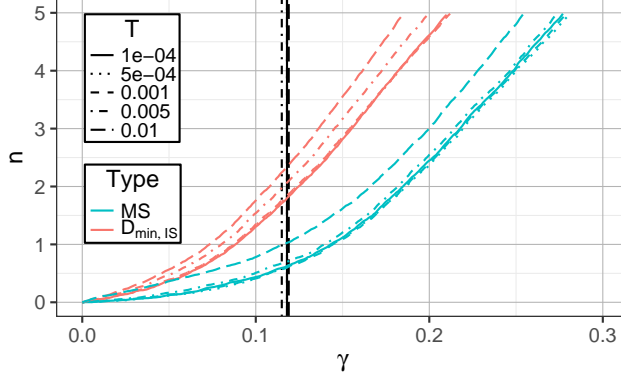


FIG. 2. Average number of MS and D_{\min} transitions since the start of the simulation. D_{\min} transitions are also used to detect IS transitions. The solid line denotes the yield strain γ_y .

fold-catastrophe occurs and the system performs a plastic event via a discontinuous change of \mathbf{x}_{IS} . This corresponds to an IS transition. In our example, this happens at $\gamma \approx 4.3$.

In addition to the IS we additionally define a minimized structure (MS). Starting from the present configuration, we minimize $V(\mathbf{x}, \gamma)$ [26]. This is comparable to an AQS simulation along the γ -direction for which the energy decreases and stopping when the potential energy displays a minimum. Since the stress at the IS is given by $\sigma = \frac{\partial}{\partial \gamma} V(\mathbf{x}_{\text{IS}}, \gamma)$, the stress at the MS is always zero. After a jump in the IS trajectory, the new IS may still be connected to the same MS, as exemplified in FIG. 1a.

The same behavior is also shown for an actual trajectory; see FIG. 1b and FIG. 1c. The increase of the IS energy ϵ_{IS} as well as the stress is interrupted by drops due to vanishing energy minima, reflecting plastic events. However, there are several plastic events where the system is still connected to the same MS. To detect IS transitions, we found that a peak detection of the minimized non-affine D_{\min} distance [27] between adjacent points in the trajectory ($\Delta\gamma = 0.001$) works best.

When averaging over many different trajectories, one can determine the average number of MS and IS transitions until some strain γ ; see FIG. 2. Note that at the strain of the overshoot maximum on average two plastic events (IS transitions) have occurred but, on average, just half a MS transition.

The first MS transition.

We start to study the properties of the first MS transition as a function of the strain γ_{MS}^1 at which this transition occurs. Specifically, we analyse the change in MS energy and in

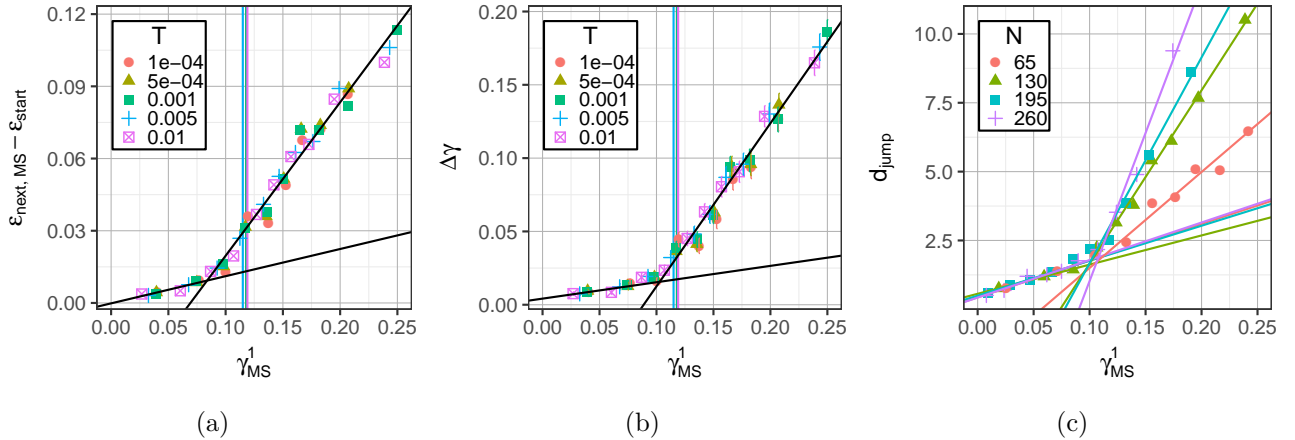


FIG. 3. Change of MS-properties after the first MS-transition as function of γ_{MS}^1 , i.e. the strain, where this transition occurs. Included are linear fits for $\gamma_{\text{MS}}^1 \leq 0.05$ and $\gamma_{\text{MS}}^1 \in [0.1, 0.2]$. The vertical lines in (a) and (b) show the position of the yield strain. (a) Change in MS energy. Intersection point: $\gamma_{\text{MS}}^1 = 0.08$. (b) Change in MS strain. Intersection point: $\gamma_{\text{MS}}^1 = 0.10$. (c) Euclidean distance between first and second MS. Intersection point: $\gamma_{\text{MS}}^1 = 0.10$.

strain as well as the Euclidean distance between the first and the second MS configuration. Remarkably, all three observables display two distinct regimes with respect to the value of γ_{MS}^1 , see FIG. 3, with a crossover in the strain range around $0.09 (\pm 0.01)$. This *crossover* strain is abbreviated as γ_c . For $\gamma_{\text{MS}}^1 < \gamma_c$, the MS properties hardly change. In contrast, for $\gamma_{\text{MS}}^1 > \gamma_c$ the dependence on γ_{MS}^1 is much stronger. In the considered low-temperature regime $T \leq 0.01$ no dependence on temperature can be seen. Additional information can be gained from studying finite-size effects as exemplary shown for the Euclidean distance in FIG. 3c. No finite-size effects are present for $\gamma_{\text{MS}}^1 < \gamma_c$, whereas for $\gamma_{\text{MS}}^1 > \gamma_c$ the distance increases with increasing system size in the range of studied system sizes. Thus the first MS transition is very localized for $\gamma_{\text{MS}}^1 < \gamma_c$ and spatially extended otherwise.

These results suggest that the few MS transitions, occurring for $\gamma < \gamma_c$ are irrelevant. This highlights the very stable, elastic structure of the glassy system, which is, apart from minor local rearrangements, robust against small perturbations. In contrast, for $\gamma > \gamma_c$ the system performs relevant irreversible MS transitions. This is exactly the physical interpretation of the critical strain γ_{nl} , extracted from the oscillatory simulations.

We can also gain insight into the emergence of the yield strain γ_y and rationalize why $\gamma_c < \gamma_y$. Since MS transitions for $\gamma < \gamma_c$ are irrelevant, we define $\tilde{\gamma}_{\text{MS}}^1$ as the first MS transition for

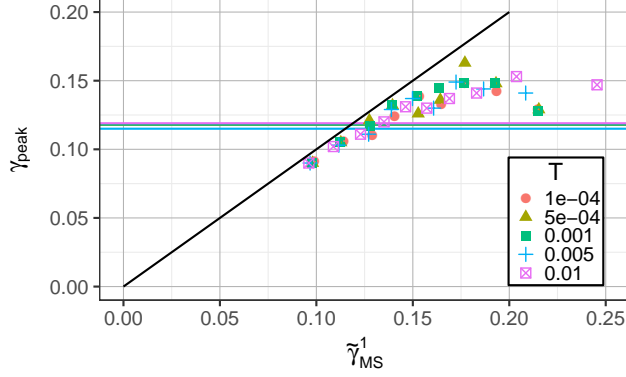


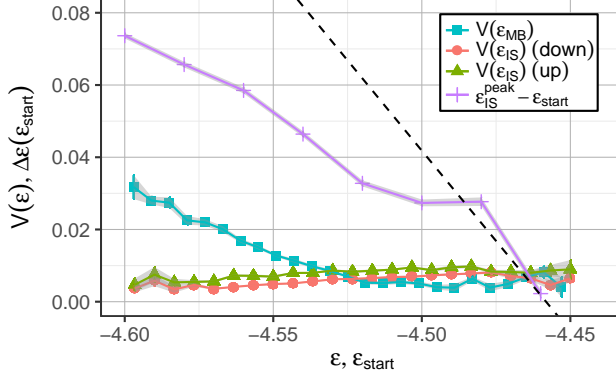
FIG. 4. Average stress overshoot peak position for all trajectories with the MS transition at a given strain. The solid black line reflects the diagonal.

$\gamma > \gamma_c$. For the large majority of transitions one has $\tilde{\gamma}_{\text{MS}}^1 = \gamma_{\text{MS}}^1$; see FIG. 2. After binning the individual stress-strain curves (like the example in FIG. 1c) for trajectories with similar values of $\tilde{\gamma}_{\text{MS}}^1$ one can determine the yield strain γ_{peak} for this subset of trajectories. These preaveraged curves can be found in [28].

FIG. 4 shows the dependence of γ_{peak} on $\tilde{\gamma}_{\text{MS}}^1$. In more than half of the trajectories one finds $0.09 < \tilde{\gamma}_{\text{MS}}^1 < 0.15$. This regime is particularly interesting because of a close similarity of γ_{peak} and $\tilde{\gamma}_{\text{MS}}^1$, seen in our simulations. Thus, it is the first MS transition which determines the yielding point. Actually, also for the rare cases for which $\tilde{\gamma}_{\text{MS}}^1 > 0.15$ there is a significant stress drop, induced by the first MS transition. However, due to the agglomeration of preceding IS transitions there is already a weak decay of the stress for $\gamma < \tilde{\gamma}_{\text{MS}}^1$; see [28]. It is also shown in [28], that MS transitions for $\gamma < 0.09$ have hardly any impact on the final stress overshoot.

Relevant barriers for yielding.

As recalled above, in the quiescent case the PEL has two hierarchy levels, namely IS and MB, giving rise to IS-IS and MB-MB transitions at finite temperatures. The transitions between MB govern the irreversible relaxation of the system above the glass transition. The typical barriers of IS-IS transitions $V(\epsilon_{\text{IS}})$ and of MB-MB transitions $V(\epsilon_{\text{MB}})$, respectively, are shown in FIG. 5a as a function of the respective energies. They have been determined by simulations at different temperatures using Arrhenius fits on the IS and MB lifetimes $\langle \tau | \epsilon_{\text{MB}}; T \rangle$ [21]. Note that $V(\epsilon_{\text{MB}})$ depends linearly on the metabasin energy ϵ_{MB} for $\epsilon_{\text{MB}} \leq -4.52$. As a consequence, the PEL can be regarded as an assembly of traps with similar absolute



(a)

FIG. 5. IS and MB activation energies for $N = 130$ particles calculated from $\langle \tau | \epsilon; T \rangle$. The activation energy for jumps to a higher/lower energetic IS is denoted by "IS up" and "IS down", respectively. The dashed line shows the difference between the mean IS energy in the flow regime $\epsilon_{\text{IS}}^{\text{flow}}$ and ϵ_{start} .

barrier energy but different trap depths ϵ_{MB} [21, 29]. In marked contrast, $V(\epsilon_{\text{IS}})$ is basically independent of the initial IS-energy.

Naturally, by applying shear to the energy landscape, not only the basins are tilted, but also the whole metabasins. Intuitively, one might relate yielding to a crossing of a MB barrier rather than an IS barrier because in analogy to the MB transitions in the quiescent case, yielding reflects an irreversible relaxation process. To analyse this question, we study how the IS energy at the yielding point $\epsilon_{\text{IS}}^{\text{peak}}$ depends on the initial starting energy ϵ_{start} by plotting $\epsilon_{\text{IS}}^{\text{peak}} - \epsilon_{\text{start}}$ vs. ϵ_{start} ; see FIG. 5a. The similarity with the energy dependence of the MB activation energies is striking. Apart from a constant shift, this similarity encompasses the linear behavior for $\epsilon_{\text{start}} \leq -4.52$ with a similar slope as well as the plateau behavior for higher energies. Naturally, this plateau stops as soon as the IS energy at the overshoot peak approaches the average IS energy in the flow regime. In contrast, no similarity exists with the energy dependence of the IS barriers. Thus, yielding involves transitions between the superstructures of the PEL, as captured by the concept of metabasins.

Discussion and Summary. The framework of the PEL $V(\mathbf{x})$ can be used for a systematic analysis of quiescent glass-forming systems. By considering the extended PEL $V(\mathbf{x}, \gamma)$ and incorporating the new concept of minimized states (MS), one can also capture the underlying properties of yielding. Irreversible MS transitions are relevant and delocalized above a

crossover strain γ_c . This strain value can be related to the onset of irreversible behavior as seen in repeated oscillatory strain simulations. Furthermore, the yielding event is clearly related to the first relevant MS transition. Thus, we can relate the observation of yielding to properties of the extended PEL $V(\mathbf{x}, \gamma)$. Finally, we observed a strong relation between the irreversible relaxation in the quiescent thermal case and yielding in the sheared athermal system.

For the PEL analysis it was important to study relatively small systems which, however, already reproduce, the yield strain also of larger systems. The plastic events, described in this work, can be considered as the elementary events, governing also the properties of larger systems via strong elastic coupling, giving rise to avalanches [1].

REFERENCES

* Corresponding author: blankburian@wwu.de

- [1] P. Leishangthem, A. D. S. Parmar, and S. Sastry, *Nat. Commun.* **8**, 14653 (2017).
- [2] G. P. Shrivastav, P. Chaudhuri, and J. Horbach, *J. Rheol.* **60**, 835 (2016).
- [3] G. P. Shrivastav, P. Chaudhuri, and J. Horbach, *Phys. Rev. E* **94**, 042605 (2016).
- [4] A. K. Dubey, I. Procaccia, C. A. Shor, and M. Singh, *Phys. Rev. Lett.* **116**, 085502 (2016).
- [5] P. K. Jaiswal, I. Procaccia, C. Rainone, and M. Singh, *Phys. Rev. Lett.* **116**, 085501 (2016), 1601.02196.
- [6] N. V. Priezjev, *Phys. Rev. E* **95**, 023002 (2017).
- [7] N. Koumakis, M. Laurati, A. R. Jacob, K. J. Mutch, A. Abdellali, A. B. Schofield, S. U. Egelhaaf, J. F. Brady, and G. Petekidis, *J. Rheol.* **60**, 603 (2016).
- [8] D. V. Denisov, M. T. Dang, B. Struth, A. Zaccone, G. H. Wegdam, and P. Schall, *Sci. Rep.* **5**, 14359 (2015).
- [9] G. Parisi, I. Procaccia, C. Rainone, and M. Singh, *Proceedings of the National Academy of Sciences*, 201700075 (2017), 1701.01019v2.
- [10] D. Fiocco, G. Foffi, and S. Sastry, *Phys. Rev. E* **88**, 020301 (2013), 1302.6518.
- [11] E. D. Knowlton, D. J. Pine, and L. Cipelletti, *Soft Matter* **10**, 6931 (2014).
- [12] T. Kawasaki and L. Berthier, *Phys. Rev. E* **94**, 022615 (2016).
- [13] W. Kob and H. C. Andersen, *Phys. Rev. Lett.* **73**, 1376 (1994), 9407118.

- [14] D. L. Malandro and D. J. Lacks, *J. Chem. Phys.* **110**, 4593 (1999).
- [15] A. W. Lees and S. F. Edwards, *J. Phys. C Solid State Phys.* **5**, 1921 (1972).
- [16] D. J. Evans and O. P. Morriss, *Computer Physics Reports* **1**, 297 (1984).
- [17] S. Sastry, P. G. Debenedetti, and F. H. Stillinger, *Nature* **393**, 554 (1998).
- [18] F. H. Stillinger and T. A. Weber, *Phys. Rev. A* **28**, 2408 (1983).
- [19] F. H. Stillinger, *Science* **267**, 1935 (1995).
- [20] B. Doliwa and A. Heuer, *Phys. Rev. E* **67**, 031506 (2003), 0209139.
- [21] A. Heuer, *J. Phys.: Condens. Matter* **20**, 373101 (2008).
- [22] K. Martens, L. Bocquet, and J.-L. Barrat, *Soft Matter* **8**, 4197 (2012), arXiv:1111.0581v2.
- [23] C. Rehwald and A. Heuer, *Phys. Rev. E* **86**, 051504 (2012).
- [24] C. E. Maloney and D. J. Lacks, *Phys. Rev. E* **73**, 061106 (2006).
- [25] Y. G. Chung and D. J. Lacks, *J. Polym. Sci., Part B: Polym. Phys.* **50**, 1733 (2012).
- [26] More precise, we first minimize $V(\mathbf{x}, \gamma = \text{const})$, which gives us \mathbf{x}_{IS} . Then we minimize $V(\mathbf{x}_{\text{IS}} + S(\gamma)\mathbf{x}_{\text{IS}} + \Delta\mathbf{x}, \gamma)$ with $\mathbf{x}_{\text{IS}} = \text{const}$ and using the shear matrix $S(\gamma)$.
- [27] M. L. Falk and J. S. Langer, *Phys. Rev. E* **57**, 7192 (1998), 9712114.
- [28] See Supplemental Material at [URL will be inserted by publisher] for more details.
- [29] J.-P. Bouchaud and G. Biroli, *Phys. Rev. B* **72**, 064204 (2005).

SUPPLEMENTAL MATERIAL FOR: METABASIN ANALYSIS OF THE STRESS OVERSHOOT IN SHEARED SUPERCOOLED LIQUIDS

Detecting IS transitions. We detect the IS jumps by finding peaks in the D_{\min} value for the IS trajectory. We found that using a peak detection algorithm works better than using a simple threshold. Also, we use D_{\min} instead of stress or energy jumps because more than 94% of the D_{\min} jumps are also stress and energy jumps, while the ratio for both other jump types are 70-80%. Peaks in the distance between successive configurations are strongly correlated to D_{\min} jumps, but the correlation to stress and energy jumps is slightly worse. The exact values can be seen in TABLE. I.

Comparison of IS and MS transitions. MS transitions are basically a subset of the IS transitions. The main difference is an additional change in the MS energy value at the transition. This makes this transition irreversible by straining in the opposite direction. However, there is an additional difference, which can be seen in FIG. 1. For D_{\min} jumps the distribution of stress values σ_{next} after the transition, has a very strong peak near the stress before the transition σ_{end} . Compared to the stresses at MS transitions the width of the distribution is small. Starting at high σ_{end} , there is only a low probability reaching stresses at or below the flow regime ($\sigma \leq 0.7$). So D_{\min} jumps are unlikely to show large stress drops, which explains the long plateau in FIG. 5c. In contrast, MS jumps show a broad distribution of σ_{next} centered around the mean stress of the flow regime, hinting at a large redistribution of stresses in the system, basically losing much of the previous stress

$P(X Y)$	d	D_{\min}	ϵ	σ
d		0.994	0.75	0.86
D_{\min}	0.90		0.70	0.81
ϵ	0.92	0.94		0.84
σ	0.90	0.94	0.73	

TABLE I. Probabilities that a jump of type X is detected at the position of a jump of type Y in the IS trajectory. X is given in horizontal and Y in vertical direction. (d : euclidean distance of all particles, D_{\min} : non-affine displacement of neighboring particles, ϵ : energy, σ : stress).

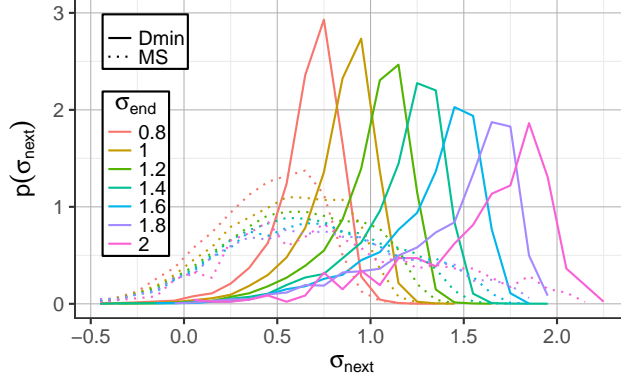


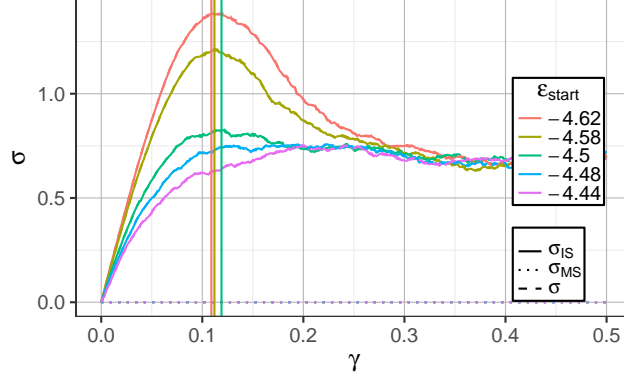
FIG. 1. Probability density $p(\sigma_{\text{next}}|\sigma_{\text{end}})$. The stress before the D_{min}/MS transition is called σ_{end} and the stress after the transition σ_{next} . To calculate the probabilities, we used all transitions with $\gamma \leq 1.0$, including both the overshoot region and the flow regime.

history. For σ_{end} smaller than the flow stress, this distinction starts to break down, as both distributions show more overlap.

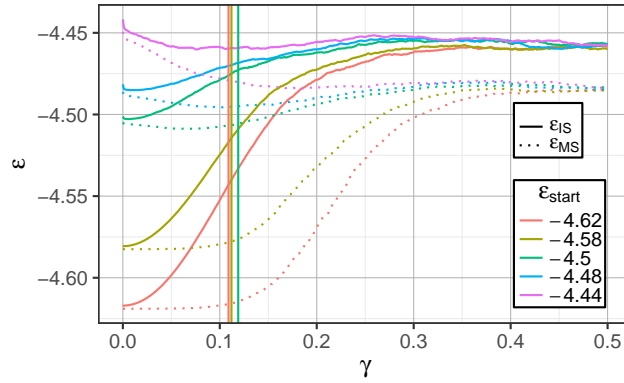
Energy and Stress during the Overshoot. The ensemble averaged stress in FIG. 2a shows the usual stress overshoot for starting energies $\epsilon_{\text{start}} \leq -4.5$ and no difference between the stress calculated from points in the trajectory and the IS stress. The maximum of the stress overshoot is around $\gamma_{\text{peak}} = 0.11$ and has no dependence on ϵ_{start} for this energy range. This is in strong contrast to γ_c , which changes with the starting energy ϵ_{start} , as can be seen in FIG. 3. We argue that this behavior is caused by an interplay of two different mechanisms. As γ_c is higher for smaller ϵ_{start} , one would expect the maximum to occur at a later point than at higher ϵ_{start} . On the other hand, having high γ_c also makes stress relaxations within the first MS more likely. However, this causes a flattening of the stress-strain curve as well as a small overshoot, as shown in FIG. 5c. In combination this results in a similar overshoot position for both low and high ϵ_{start} .

For $\epsilon_{\text{start}} \geq -4.5$, we see no pronounced stress overshoot. The stress maximum therefore shifts to higher γ and marks the position where we enter the flow regime. At all MS the stress is approximately zero ($|\sigma_{\text{MS}}| < 2 \cdot 10^{-5}$), because the stress is connected to the energy via $\sigma = \frac{\partial V(\epsilon, \gamma)}{\partial \gamma}$.

In FIG. 2b the MS energies change very little up until $\gamma \approx 0.09$ for all $\epsilon_{\text{start}} \leq -4.5$. This behavior is in accord with FIG. 3, which shows the MS energies after the first MS transition for different ϵ_{start} . So for all $\epsilon_{\text{start}} \leq -4.5$, we have similar energies for $\gamma_{\text{MS}} \leq 0.07$, but what



(a) Stress



(b) Energy

FIG. 2. Ensemble averaged (a) energy and (b) stress. Solid lines represent IS energies/stresses and dotted lines MS energies/stresses. Vertical lines show the position of the maximum of the stress overshoot for the respective starting energy.

changes dramatically is the slope of ϵ_{IS} .

First minimized structure. As shown in the main text for the low starting energy of $\epsilon_{\text{start}} = -4.6$ the change in MS energy is very small for $\gamma_{\text{MS}}^1 \leq 0.09$, giving rise to the notion of irreversible MS transitions for $\gamma_{\text{MS}}^1 > 0.09$. As seen in FIG. 3 this holds for all starting energies $-4.64 \leq \epsilon_{\text{start}} \leq -4.5$. Naturally, the cutoff is not that pronounced at high energies, because of a smaller change in slope.

Furthermore, the dependence of the peak position γ_{peak} on $\tilde{\gamma}_{\text{MS}}^1$ is also identical for all starting energies, finding three different regions (FIG. 4a). For small $\tilde{\gamma}_{\text{MS}}^1$, we see some high outliers, which are reminiscent of the point cloud seen at $\gamma_{\text{MS}}^1 \leq 0.09$. For completeness, we also plot the full range of γ_{MS}^1 in FIG. 4b, which also shows γ_{peak} for small γ_{MS}^1 .

The values for $\tilde{\gamma}_{\text{MS}}^1 \leq 0.07$ show, that there is no correlation between the peak position and

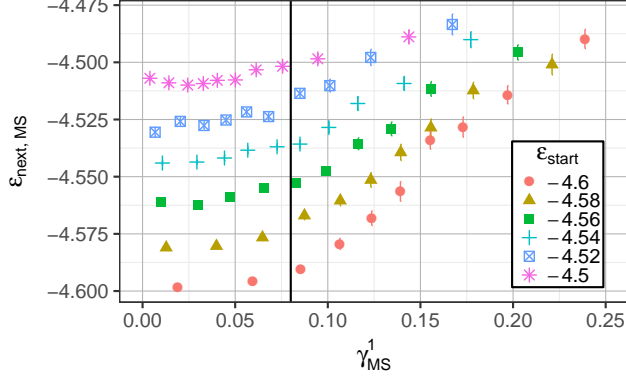
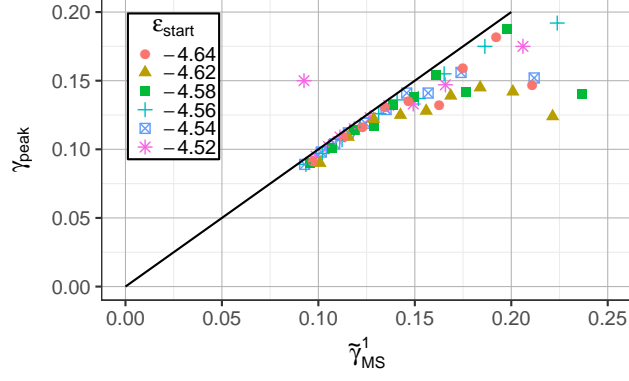


FIG. 3. Averaged MS energy directly following the first MS-transition at $\tilde{\gamma}_{\text{MS}}^1$. As a guide for the eye, the vertical line marks $\gamma = 0.09$.

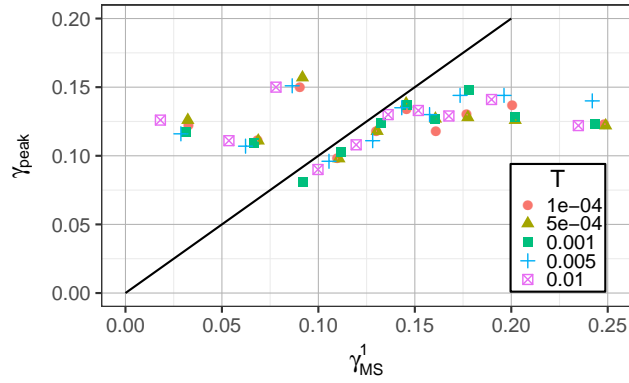
the first MS jump in this regime. In FIG. 5a, some sub-ensembles from trajectories in this region are shown. One can see, that for each sub-ensemble, the stress resembles closely the ensemble average over all trajectories. This means, that these transitions have no special contribution to the stress overshoot.

In the region $0.09 \leq \tilde{\gamma}_{\text{MS}}^1 \leq 0.2$ (FIG. 5c) we see that there is a large stress drop in each sub-ensemble. The stress drop occurs sharply at or slightly after the peak position. The shift can be explained by small IS transitions, which may happen before the MS transition.

The trajectories for the region $\tilde{\gamma}_{\text{MS}}^1 > 0.2$ are shown in FIG. 5c. We observe that all trajectories start with a slightly negative stress. Since we simulate a small system with fixed boundary conditions the stress after minimizing the potential energy may be non-zero, also in the fully equilibrated system. This leads to a slight γ offset to the ensemble average until the point where we see a plateau. This plateau is almost as high as the ensemble average, so it is built by small stress drops, which cancel out in the sub-ensemble. The stress is kept high because of the high energy difference between the low energetic MS energy and the current already high IS energy after the small stress drops. The plateau then ends with a sudden drop in stress, which is caused by a large stress released together with the MS transition.



(a)



(b)

FIG. 4. Average stress overshoot peak position γ_{peak} for all trajectories with the first MS transition at a given strain, plotted for (a) different starting energies and (b) different small temperatures. In (a) we use the first MS transition with $\gamma_{\text{MS}} \geq 0.09$ and in (b) we use the first MS transition.

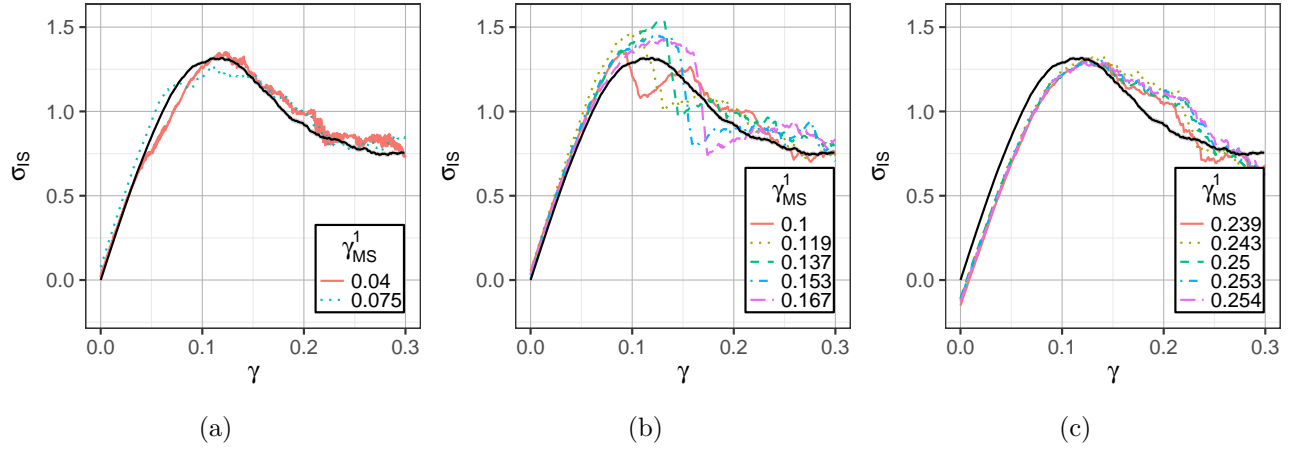


FIG. 5. a) Stress of sub-ensembles with a given strain $\gamma_{MS} < 0.09$. Show are trajectories for temperatures $T \in \{1 \cdot 10^{-4}, 5 \cdot 10^{-4}\}$. b) The same for $\gamma_{MS} \in (0.09, 0.2)$ and $T = 10^{-4}$. c) For $\gamma_{MS} > 0.21$ we plot all available values for $T \in [10^{-4}, 10^{-2}]$.